Journal of Computational Physics **152,** 359–384 (1999)
Article ID jcph.1999.6251, available online at http://www.idealibrary.com on IDEAL®

Iterative Convergence Acceleration of Neutral Particle Transport Methods via Adjacent-Cell Preconditioners

Y. Y. Azmy

Oak Ridge National Laboratory, P.O. Box 2008, MS 6363, Oak Ridge, Tennessee 37831-6363
E-mail: yya@ornl.gov, Fax: (423) 574-9619

Received December 22, 1997; revised December 15, 1998

We propose preconditioning as a viable acceleration scheme for the inner iterations of transport calculations in slab geometry. In particular we develop Adjacent-Cell Preconditioners (AP) that have the same coupling stencil as cell-centered diffusion schemes. For lowest order methods, e.g., Diamond Difference, Step, and 0-order Nodal Integral Method (0NIM), cast in a Weighted Diamond Difference (WDD) form, we derive AP for thick (KAP) and thin (NAP) cells that for model problems are unconditionally stable and efficient. For the First-Order Nodal Integral Method (1NIM) we derive a NAP that possesses similarly excellent spectral properties for model problems. [Note that the order of NIM refers to the truncated order of the local expansion of the cell and edge fluxes in Legendre series.] The two most attractive features of our new technique are: (1) its cell-centered coupling stencil, which makes it more adequate for extension to multidimensional, higher order situations than the standard edge-centered or point-centered Diffusion Synthetic Acceleration (DSA) methods; and (2) its decreasing spectral radius with increasing cell thickness to the extent that immediate pointwise convergence, i.e., in one iteration, can be achieved for problems with sufficiently thick cells. We implemented these methods, augmented with appropriate boundary conditions and mixing formulas for material heterogeneities, in the test code AP1D that we use to successfully verify the analytical spectral properties for homogeneous problems. Furthermore, we conduct numerical tests to demonstrate the robustness of the KAP and NAP in the presence of sharp mesh or material discontinuities. We show that the AP for WDD is highly resilient to such discontinuities, but for 1NIM a few cases occur in which the scheme does not converge; however, when it converges, AP greatly reduces the number of iterations required to achieve convergence.

Key Words: preconditioning; adjacent-cell preconditioner; neutral particle transport; spectral analysis.

0021-9991/99

I. INTRODUCTION

The slow convergence of Source Iterations (SI) traditionally employed in solving neutral particle (neutrons and photons) transport problems in the diffusive regime prompted the search for efficient acceleration schemes. Among these, the Diffusion Synthetic Acceleration (DSA) method was initially attractive because it was believed that standard, highly efficient, cell-centered codes based on diffusion theory could be attached simply as an acceleration module to *any* transport code. It was not long until this plan, not DSA per se, failed in some cases [1], in fact primarily the cases most in need of acceleration in the first place. The conditional stability of DSA for accelerating the Diamond Difference (DD) method, the dominant method of the time, was proved through the analysis by Reed of a model configuration, i.e., an infinite row of identical cells [1]. This behavior was later articulated in *Alcouffe's Consistency Principle*, which states that a necessary condition for stability and efficiency of a DSA scheme is the *consistency* between the discrete-variable forms of the diffusion and transport operators involved [2]. However, the nature of this consistency, and a systematic approach to deriving the discrete-variable DSA equations remained unspecified until Larsen interpreted consistency in the *derivational* sense and prescribed the Four Step Method (FSM) as a means of deriving an unconditionally stable and efficient DSA [3]. He demonstrated FSM for several spatial approximations in slab geometry [3]; then McCoy and Larsen verified the predicted spectral properties for model, as well as non-model, problems [4].

Research into acceleration methods has not ceased since then and has been motivated primarily by the following considerations:

1. The difficulty of the FSM–DSA formalism, which inhibits its extension to multidimensional or non-Cartesian geometries, higher order methods, and alternative discretization schemes, e.g., the nodal and characteristic methods. Over the years many authors have introduced simplifying assumptions to overcome this obstacle, achieving varying degrees of success.
2. A nonstandard edge-centered form of the FSM–DSA acceleration equation, which in multidimensional cases requires solving a discrete-variable problem larger than that solved by cell-centered schemes that have been studied, analyzed, and tested more comprehensively.
3. The potential for achieving spectral properties better than those achieved by the FSM–DSA.

A cell-centered scheme, which resembles to a large extent a DSA method, was proposed and successfully tested by Gelbard and Khalil for DD in slab geometry [5]. Later Khalil [6] formulated a Consistent Diffusion Differencing (CDD) acceleration technique that he showed is equivalent to FSM–DSA with S_2 angular quadrature in slab geometry, then proceeded to illustrate that it can be written in a cell-centered form. However, extension of CDD to multidimensional geometry requires simultaneously solving for the transverse-leakage discrete variables which are defined on cell edges. More recently, in an effort to better understand Reed's results, the Imposed DSA (IDSA) scheme was reported [7]. In this method a cell-centered diffusion equation with an arbitrary diffusion length is *imposed* to accelerate the 1D Weighted Diamond Difference (WDD) discrete ordinates form of the transport equation. [The WDD includes as special cases several standard methods, such as DD, the Step method, and the Zero-Order Nodal Integral Method (0NIM) [8], characterized by a single spatial parameter; the order of NIM specifies the order of the truncated Legendre

expansion of the flux as detailed in Ref. [8].] Spectral analysis of the resulting accelerated iterative process yielded the spectral radius as a function of the diffusion length and the computational cell optical thickness, for various values of the WDD spatial weights [7]. The results of this work showed that Reed's conclusion [1] regarding the failure of cell-centered schemes to accelerate thick-cell problems is strictly true for the DD method used in his analysis, but that it does not hold for large-weight WDD methods, such as Step, and also 0NIM.

The IDSA essentially legitimized the search for acceleration operators of the cell-centered diffusive type to implement with non-DD discretizations of the transport equation. In this paper we present a new approach for accelerating iterative convergence of WDD and the linear method, 1NIM [8], in slab geometry that is based on traditional preconditioning studied as a general framework in developing iterative methods for solving large problems in linear algebra [9, 10]. In contrast to the IDSA [7], here we start by considering a class of cell-centered preconditioner coupling stencils, then show that a generalized diffusion relation among the elements of the preconditioner with adjacent-cell coupling is necessary for the stability of the iterative scheme. Thus, in Section II we examine the case of WDD, a zero-order class of methods, in great detail, deriving and verifying Adjacent-Cell Preconditioners (AP) that are unconditionally stable, and whose spectral radii decrease to zero with increasing cell thickness. Due to the complexity of the first-order case, in Section III we briefly describe AP for thick cells, then examine in detail only the AP for thin cells and 1NIM, which has spectral properties that are as desirable as those of the WDD scheme. The spectral analyses conducted in Sections II and III are based on decomposing the iteration residual into Fourier modes for model problem configurations characterized by an infinite row of equal-sized computational cells with homogeneous material composition. Realistic problems of non-periodic finite extent and material heterogeneities do not permit a Fourier analysis; however, we extend the AP formalism to such cases by applying standard formulas for vacuum boundary conditions, and for mixing the preconditioner elements across mesh and material discontinuities. Numerical tests conducted with the slab geometry computer code AP1D are included in both Section II and Section III to verify this extension of the spectral analysis results, and to facilitate examination of the effect of material and mesh discontinuities on the efficiency of the AP. A brief summary of this work and our main conclusions are included in Section IV.

II. ACCELERATION OF THE WDD

The most general form of the WDD form of the one-group, steady state, discrete ordinates approximation of the neutron transport equation in slab geometry comprises two sets of relations. The first set is a per cell statement of balance of sources and *sinks* of neutrons

$$\varepsilon_{n,j}\left[\tilde{\psi}^{o,l'}_{n,j}-\tilde{\psi}^{i,l'}_{n,j}\right]+\tilde{\psi}^{l'}_{n,j}=c_j\tilde{\phi}^{l}_{j}+s_j, \qquad n=1,\ldots,N;\ j=1,\ldots,J, \tag{1.a}$$

where l and l' denote the previous and present inner iterations, respectively; $\tilde{\psi}^{l'}_{n,j}$ is the present iterate of the nth angular flux averaged over cell j; $\tilde{\psi}^{o,l'}_{n,j}$ and $\tilde{\psi}^{i,l'}_{n,j}$ are the present iterates of the nth angular flux evaluated at the outgoing and incoming edges of cell j, respectively; $\tilde{\phi}^{l}_{j}$ is the previous iterate of the scalar flux averaged over cell j; s_j is the fixed source averaged over cell j; the reciprocal of half the optical thickness of cell j is defined

as

$$\varepsilon_{n,j} \equiv \frac{2|\mu_n|}{\sigma_j a_j}; \tag{1.b}$$

μ_n is the nth discrete direction; σ_j is the macroscopic total cross section in cell j; a_j is the size of cell j; and c_j is the scattering ratio in cell j. Equation (1.a) is exact in the sense that it is obtained by direct integration of the continuum transport equation and using standard definitions of the cell-average flux and source. The terms on the left hand side of Eq. (1) represent the loss of neutrons from cell j by streaming, and collisions, while the terms on the right hand side (RHS) represent the sources from isotropic scattering, and external fixed sources, respectively.

The second set of equations in a generic WDD form of the discrete-variable transport equation provides an additional weighted-difference relation between the cell-average and cell-edge flux variables

$$\tilde{\psi}^{l'}_{n,j} = \left(\frac{1+\alpha_{n,j}}{2}\right)\tilde{\psi}^{o,l'}_{n,j} + \left(\frac{1-\alpha_{n,j}}{2}\right)\tilde{\psi}^{i,l'}_{n,j}, \qquad n = 1, \ldots, N;\ j = 1, \ldots, J. \tag{2}$$

The dependence of the spatial weights $\alpha_{n,j} \in [0, 1]$ on problem parameters is determined by the formalism of the underlying numerical method or simplifying assumptions applied directly to Eq. (2). For example, DD corresponds to

$$\alpha_{n,j} = 0, \tag{3.a}$$

equivalent to expanding the flux within cell j in a Legendre series truncated at order two. The Step method assumes a thick cell where the exponential decay of the incoming cell-edge flux causes it to dominate the cell-average flux, hence

$$\alpha_{n,j} = 1. \tag{3.b}$$

The 0NIM is the lowest order member of a class of methods whose order denotes the truncation order of Legendre expansions of the flux within each cell, and in multidimensional cases on cell edges also [8]. The spatial weights for the 0NIM are given by [8]

$$\alpha_{n,j} = \coth(1/\varepsilon_{n,j}) - \varepsilon_{n,j}. \tag{3.c}$$

Solving Eqs. (1.a) and (2) for a given cell-average scalar flux, i.e., initial guess or previous iterate, along one discrete ordinate over the entire mesh is typically conducted via the "mesh-sweep" algorithm, which amounts to the following. The starting cell for each angle μ_n is one with an external boundary where the incoming flux is explicitly (e.g., vacuum boundary condition) or implicitly specified in terms of the outgoing flux at this boundary (reflective, albedo, or periodic boundary conditions). The incoming flux in Eqs. (1.a) and (2) is set to the prescribed value if an explicit boundary condition is specified, or to a previously computed outgoing flux otherwise, i.e., mesh sweep along $-\mu_n$ or previous iterate when iterations on the boundary condition are necessary. The mesh sweep then proceeds by recursively solving Eqs. (1.a) and (2) simultaneously for the cell-average flux and outgoing cell-edge flux, assigning the latter to the incoming cell-edge flux of the adjacent down-stream cell (angular flux continuity across cell edges) and repeating the process. Upon completion of

the mesh sweep for all discrete ordinates the scalar flux is updated as described shortly and convergence is tested; this constitutes a single inner iteration.

For the purpose of the ensuing spectral analysis it is convenient to write the equations for the WDD in homogeneous form by subtracting the set of equations in two consecutive iterations, thus eliminating the fixed source, s_j, and replacing the dependent discrete variables by their iterative residual counterparts. Accordingly, the most general WDD form of the discrete-ordinates approximation to the transport equation can be written in matrix form,

$$\mathbf{T}^0_{n,j}\left[\psi^{l'}_{n,j}, \psi^{o,l'}_{n,j}\right]^T = \mathbf{S}^0_{n,j}\left[\phi^l_j, \psi^{i,l'}_{n,j}\right]^T, \qquad n = 1, \ldots, N;\ j = 1, \ldots, J, \tag{4}$$

where, for example $\psi^{l'}_{n,j} \equiv \tilde{\psi}^{l'}_{n,j} - \tilde{\psi}^{l'-1}_{n,j}$ is the mesh-sweep residual in the nth angular flux averaged over cell j, and so on. The superscript on the matrices in Eq. (4) denotes the lowest order WDD method; it follows directly from Eqs. (1.a) and (2) that

$$\mathbf{T}^0_{n,j} \equiv \begin{bmatrix} 1 & \frac{\varepsilon_{n,j}}{2} \\ 1 & -\frac{1+\alpha_{n,j}}{2} \end{bmatrix}, \tag{5.a}$$

$$\mathbf{S}^0_{n,j} \equiv \begin{bmatrix} c_j & \frac{\varepsilon_{n,j}}{2} \\ 0 & \frac{1-\alpha_{n,j}}{2} \end{bmatrix}, \tag{5.b}$$

Closure of the iterative process represented in Eq. (4) by the indices l and l' is accomplished in the SI scheme by setting

$$\phi^{l+1}_j = \phi^{l'}_j = \sum_{n=1}^{N} w_n \psi^{l'}_{n,j}, \tag{6}$$

where w_n are the weights associated with the angular quadrature. Acceleration schemes aim at replacing Eq. (6) with an alternative updating formula that results in faster convergence. We start this section with a brief outline of the preconditioning method as it applies to neutral particle transport methods in general, and justify the diffusion coupling stencil for the preconditioner. Then we devise prescriptions for the preconditioner parameters for thin and thick computational cells separately, and following this we give formulas for mixing the preconditioner parameters across material discontinuities, and for the boundary conditions. We close the present section by verifying the spectral analysis on a set of model and non-model test problems, confirming the rapid convergence of the preconditioned iterations, even in the presence of sharp material discontinuities.

II.1. Preconditioning Neutral Particle Transport Methods

The standard mesh-sweep algorithm commonly used in solving the discretized integro-differential form of the discrete-ordinates approximation of the neutron transport equation is focused on the discrete-variable angular flux as demonstrated by Eq. (4). Considering the linearity of Eq. (4) and the quadrature formula, Eq. (6), then composing the mesh-sweep operator with the summation operator over angles can be viewed as a mapping of the scalar flux accomplished via

$$\phi^{l'} = \mathbf{A}(\sigma_s \phi^l + S), \tag{7}$$

In Eq. (7), $\mathbf{A}$ is the iteration Jacobian matrix; $\phi^{l'}$ and ϕ^{l} are vectors of the old and new iterates of the cell-average scalar flux residual, respectively, each of length J, the number of computational cells in 1D slab geometry; σ_s is a diagonal matrix whose nonzero elements are the J macroscopic scattering cross sections; and S is a J-vector of the cell-average fixed neutral particle source. Matrix $\mathbf{A}$ represents the inverse of the discrete streaming operator integrated (or summed) over all angular directions. A standard theorem in linear algebra [9] is that the convergence of the iterative scheme comprising Eq. (7) plus Eq. (6) is determined by the spectral radius of $\sigma_s\mathbf{A}$. It is a classical result in neutron transport numerical methods that these iterations converge slowly in highly scattering, optically thick systems [1–3].

In general, if the iterations, Eqs. (7) and (6), converge to the limit ϕ^{∞}, then

$$\mathbf{B}\phi^{\infty} = \mathbf{A}S, \tag{8}$$

where

$$\mathbf{B} = \mathbf{I} - \mathbf{A}\sigma_s, \tag{9}$$

and $\mathbf{I}$ is the J-dimensional identity matrix. Had it been possible to construct and invert (or factor) matrix $\mathbf{B}$, the transport problem would have been immediately solvable without iterations [11, 12]. However, for most practical applications this proposition is inadequate, and a *splitting* of $\mathbf{B}$ to perform the iterations is inevitable. In particular, one can apply the splitting

$$\mathbf{B} \equiv \mathbf{D} - (\mathbf{D} - \mathbf{B}), \tag{10}$$

with $\mathbf{D}$ selected to be easily invertible, then define the iterative scheme by

$$\mathbf{D}\phi^{l+1} = (\mathbf{D} - \mathbf{B})\phi^{l} + \mathbf{A}S. \tag{11}$$

In this case $\mathbf{D}$ is called the *preconditioner*, and Eq. (11) is the preconditioned system. Using Eqs. (7) and (9) in Eq. (11), one obtains

$$\phi^{l+1} - \phi^{l} = \mathbf{D}^{-1}(\phi^{l'} - \phi^{l}), \tag{12}$$

where $\phi^{l'}$ is the mesh-sweep scalar flux; see Eq. (7). Notice that if $\mathbf{D}$ is not singular then convergence of the mesh-sweep flux, i.e., $\phi^{l'} = \phi^{l}$, implies convergence of the preconditioned flux to the same solution, $\phi^{l+1} = \phi^{l}$. Equation (12) is more convenient for practical purposes than Eq. (11) because usually matrices $\mathbf{A}$ and $\mathbf{B}$ are too large to construct and store in memory, while $\phi^{l'}$ is readily available. While there are many similarities between the preconditioned system, Eq. (12), and standard DSA, as well as the IDSA, methods, it differs in one important respect: here the update is made relative to the previous preconditioned iterate rather than the mesh-sweep flux. The spectral analyses conducted below will demonstrate the importance of this difference in the case of thick computational cells, and will require that it be rescinded in favor of the traditional update with respect to $\phi^{l'}$ in the case of thin cells.

Evidently the selection of the preconditioner $\mathbf{D}$ bears heavily on the stability and efficiency of the preconditioned iterations represented by Eqs. (7) and (12). On the one hand a simple

choice of **D** makes the updating step, Eq. (12), computationally inexpensive but may not sufficiently reduce the number of iterations. A good example of such a choice is

$$\mathbf{D} = \mathbf{I}, \tag{13}$$

which reduces the preconditioned iterations to the SI scheme, i.e., Eqs. (7) and (6). This choice, Eq. (13), is none other than the classical Richardson iterative scheme, generally known to require a number of iterations of order J^2 to achieve convergence for a matrix equation of order J [9, 10]. This estimate for the number of iterations turns out to be too conservative for SI when $c < 1$ or the cell size decreases like $O(J^{-1})$; in such cases the number of SI iterations does not grow indefinitely but peaks or saturates as J increases, respectively. Even more sophisticated choices of the preconditioner, for example, the Jacobi Method, $\mathbf{D} = Diag(\mathbf{B})$, the Gauss–Seidel Method, $\mathbf{D} =$ Lower Triangle of **B**, or Successive over Relaxation (SOR), $\mathbf{D} =$ Lower Triangle of **B** with weighted diagonal elements, etc. which are easy to *solve*, require a number of iterations that is of the order of some power of J for **B** and **D** $J \times J$ matrices.

At the other extreme, a more complicated choice of **D** may result in a substantial reduction in the number of iterations independent of J, but end up being more costly to solve, as in Eq. (12). Examples of such preconditioners are the FSM–DSA [3] and the IDSA [7], which possess iteration spectral radii that are bounded well below unity. Even though the tridiagonal diffusion-like equation (at least in slab geometry) that must be solved at every iteration is more difficult than the mesh sweep in each discrete direction, usually it results in a net reduction of execution time, especially in high-quadrature-order problems. This beneficial effect of DSA and IDSA is projected to be even more pronounced in multidimensional geometry, due to the normally large number of discrete angles employed, even though in this case the preconditioner becomes a sparse banded matrix that must be solved iteratively itself. This conjecture is based on experience with the Partial Current Rebalance acceleration option in the TORT code [13], which employs an SOR algorithm to solve an acceleration equation that has a diffusion coupling stencil. In large applications this acceleration technique typically consumes about 5% of, while dramatically reducing, the total CPU time.

In spite of the considerable latitude permitted in selecting the preconditioner, thus the multitude of DSA formalisms in the literature, it is desirable that it satisfy at least one obvious criterion: that the slowest converging mode of the residual in the SI scheme be an eigenmode of the preconditioner also, with the corresponding preconditioner eigenvalue equal to one minus the corresponding eigenvalue of the SI operator. If this is the case, then the exact solution of the preconditioned system represented by the updating step, Eq. (12), will result in the immediate elimination of this eigenmode, and because the iterations are linear it cannot be excited again. Intuitively, if the spectrum of the preconditioned system is continuous near the slowest converging mode, then neighboring eigenmodes will also suffer attenuation of their magnitudes, thereby converging rapidly.

The similarity between DSA methodology and tridiagonal preconditioners in slab geometry raises the obvious question of how to generalize it to multidiagonal preconditioners, and how much of the **B** matrix elements to exactly include in **D**. First we show how the exact elements of **B** can be constructed up to a few off-diagonal bands for the WDD system of Eq. (4); for an algorithmic approach see Ref. [12].

To compute the elements of **A** we differentiate Eq. (7) with respect to the previous iterate residual

$$\mathbf{A}_{i,j} = \frac{1}{\sigma_{s,j}} \frac{\partial \phi_i^{l'}}{\partial \phi_j^l}. \tag{14}$$

The diagonal elements of **B** are computed by substituting Eq. (4) into Eq. (14) with i set to j, then using the result in Eq. (9) to obtain

$$\mathbf{B}^0_{j,j} = 1 - c_j \sum_{n=1}^{N} w_n \frac{1+\alpha_{n,j}}{1+\varepsilon_{n,j}+\alpha_{n,j}}. \tag{15}$$

Determining the first off-diagonal elements, e.g., $\mathbf{B}_{j,j+1}$, first requires solving Eq. (4) for $\psi^{o,l'}_{n,j}$. For $\mu_n > 0$ we use the continuity of the angular flux (and consequently that of the iteration residual) across cell edges to equate the resulting expression to $\psi^{i,l'}_{n,j+1}$. Substituting the latter into Eq. (4) at $j+1$ produces a relation between $\psi^{l'}_{n,j+1}$ and ϕ^l_j, from which we compute $\partial \psi^{l'}_{n,j+1}/\partial \phi^l_j$, $\mu_n > 0$, while clearly this derivative vanishes for $\mu_n < 0$. This leads to

$$\mathbf{B}^0_{j,j\pm1} = -c_{j\pm1} \sum_{n=1}^{N} w_n \frac{\varepsilon_{n,j}}{(1+\varepsilon_{n,j}+\alpha_{n,j})(1+\varepsilon_{n,j\pm1}+\alpha_{n,j\pm1})}, \tag{16}$$

where we have assumed symmetry of the angular quadrature: for each discrete ordinate n there is another discrete ordinate n' such that $\mu_{n'} = -\mu_n$ and $w_{n'} = w_n$. In the same way additional off-diagonal elements of **B** can be determined: for example, if we assume homogeneous cell properties

$$\mathbf{B}^0_{j,j\pm2} = -c_j \sum_{n=1}^{N} w_n \frac{\varepsilon_{n,j}(\varepsilon_{n,j}+\alpha_{n,j}-1)}{(1+\varepsilon_{n,j}+\alpha_{n,j})^3}, \tag{17}$$

and so on.

The increasing complexity of the elements of **B** as we go farther from the diagonal, even if there exist efficient algorithms for solving such multidiagonal systems, raises the important question, How many diagonal elements ought to be included? The properties of the transport operator intuitively suggest that the off-diagonal elements diminish in magnitude rapidly as they get farther from the diagonal, and that **B** becomes diagonally dominant with increasing cell optical thickness. To quantify these propositions we expand the expressions in Eqs. (15)–(17) asymptotically in the reciprocal of the cell optical thickness for a model problem to obtain

$$\mathbf{B}^0_{j,j} = 1 - c + \frac{c}{\sigma a} \sum_{n=1}^{N} w_n |\mu_n| + O(\sigma a)^{-2}, \tag{18}$$

$$\mathbf{B}^0_{j,j\pm1} = -\frac{c}{2\sigma a} \sum_{n=1}^{N} w_n |\mu_n| + O(\sigma a)^{-2}, \tag{19}$$

$$\mathbf{B}^0_{j,j\pm2} = -\frac{c}{(\sigma a)^3} \sum_{n=1}^{N} w_n |\mu_n|^3 + O(\sigma a)^{-4} = O(\sigma a)^{-3}, \tag{20}$$

where we have suppressed the cell indices on the cell properties to indicate model (homogeneous material and uniform mesh) configuration. For highly scattering problems, $c \sim 1$, Eqs. (18)–(20) imply that the diagonal and first off-diagonal elements of **B** are of the same order; hence they dominate all other elements as $\sigma a \to \infty$. Consequently, for highly scattering problems with optically thick cells a tridiagonal preconditioner will very closely approximate the full **B** matrix to the extent that the solution of the preconditioned system, Eq. (12), will sufficiently approximate the *exact* solution, thereby effecting immediate convergence of the iterations. On the other hand, for highly absorbing problems, $c \sim 0$, the diagonal elements dominate even the first off-diagonal elements by one order of magnitude so that for optically thick problems a diagonal preconditioner (Jacobi method) may be sufficient to achieve rapid convergence.

II.2. Adjacent-Cell Preconditioners for WDD

Having established the merit of tridiagonal, or adjacent-cell, preconditioners (the diffusion coupling stencil in slab geometry) in the diffusive regime, our next step is to determine preconditioner parameters that lead to unconditional convergence and efficiency of the preconditioned iterations. The dominance of the tridiagonal elements in this regime intuitively suggests that the AP elements take the form of Eqs. (15), (16). However, this prescription violates the selection criterion discussed above because it is well known that the slowest converging modes in the diffusive regime are the flat modes [3], which do not necessarily satisfy an AP with Eqs. (15), (16). Hence we seek better prescriptions for the AP elements via a spectral analysis of the iterative procedure.

First, in analogy to the homogenization process applied to Eq. (4), Eqs. (7)–(12) can be written in homogeneous form by setting S to zero and interpreting all ϕ variables as iteration residuals. Then assuming model problem configuration we decompose all iteration residuals in the computed quantities into their Fourier modes via

$$\phi_j^l = \Phi^l \exp[\hat{\imath}\lambda x_j], \tag{21.a}$$

$$\psi_{n,j}^{l'} = \Psi_n^{l'} \exp[\hat{\imath}\lambda x_j], \tag{21.b}$$

$$\psi_{n,j}^{o,l'} = \tilde{\Psi}_n^{l'} \exp[\hat{\imath}\lambda (x_j + \mathrm{sg}(\mu_n) a/2)], \tag{21.c}$$

$$\psi_{n,j}^{i,l'} = \tilde{\Psi}_n^{l'} \exp[\hat{\imath}\lambda (x_j - \mathrm{sg}(\mu_n) a/2)], \tag{21.d}$$

$$\phi_j^{l'} = \Phi^{l'} \exp[\hat{\imath}\lambda x_j], \tag{21.e}$$

where $\hat{\imath} \equiv \sqrt{-1}$, sg is the signum function, λ is the Fourier variable, and x_j is the position of the center of mass of the jth cell. Substituting Eqs. (21) into Eq. (4) yields [7]

$$\Phi^{l'} = c[1 - (\sin^2 r)\chi(r)]\Phi^l, \tag{22}$$

where we have assumed symmetry of the angular quadrature and defined

$$\chi(r) \equiv \sum_{n=1}^{N} w_n \frac{\varepsilon_n(\varepsilon_n + \alpha_n)}{\cos^2 r + (\varepsilon_n + \alpha_n)^2 \sin^2 r}, \tag{23}$$

and $r \equiv \lambda a/2$.

Using an arbitrary adjacent-cell preconditioner **D** in Eq. (12) and decomposing into Fourier modes yield the spectrum of the preconditioned iterations

$$e(r) \equiv \Phi^{l+1}(r)/\Phi^{l}(r) = \left[1 - \frac{1 - c + c(\sin^2 r)\chi(r)}{D_d + 2D_o - 4D_o \sin^2 r}\right], \tag{24}$$

where D_d, and D_o are the diagonal and off-diagonal elements of the AP, respectively.

The inadequacy of the AP with exact tridiagonal elements, i.e., Eqs. (15), (16), is now evident. Taking the limit $r \to 0$ of Eq. (24),

$$e(0) = \left[1 - \frac{1 - c}{D_d + 2D_o}\right], \tag{25.a}$$

then setting $D_d = \mathbf{B}^0_{j,j}$ and $D_o = \mathbf{B}^0_{j,j\pm1}$ yield

$$e(0) \to 1, \qquad \text{as } c \to 1. \tag{25.b}$$

A thorough examination of Eq. (25.a) with arbitrary AP elements reveals a necessary condition for the stability of the preconditioned iterations as $c \to 1$, namely

$$D_o = \frac{1}{2}\left[\frac{1 - c}{b} - D_d\right], \qquad b \in (0, 2). \tag{26}$$

This stability condition with $b = 1$ is reminiscent of the cell-centered discretization of the neutron diffusion operator where D_o is set to the square of the ratio of the diffusion length to the cell size; it results in immediate removal of the $r = 0$ eigenmode, the slowest converging SI mode. For these two reasons, in the remainder of this paper, we refer to Eq. (26) with $b = 1$, in particular, as the *stability condition*. Note that in the worst case, i.e., the trajectory $c = 1$, the value of b is inconsequential to the convergence of the $r = 0$ eigenmode. In general, the eigenvalue surface $e(r; c)$ given by Eqs. (24) and (26) is multivalued at the point $r = 0$, $c = 1$, with the limit of e depending on the trajectory of approach to this point. The limit value of e is $(1 - b)$ for all trajectories except $c = 1$.

II.2.a. *Thick-Cell AP for WDD*

In the context of model problem configurations there are only two AP parameters to be determined, D_d and D_o. In view of the stability condition, Eq. (26), we are free to choose only one more condition for the spectrum to satisfy: we require the limit of Eq. (24) to vanish as $r \to 0$. The $O(r^0)$ term vanishes by virtue of Eq. (26) with $b = 1$; the $O(r^2)$ terms, which are the most significant terms when $c = 1$, provide an expression for D_o which when combined with Eq. (26) yields

$$D_d = \frac{c}{2}\sum_{n=1}^{N} w_n \varepsilon_n (\varepsilon_n + \alpha_n), \tag{27}$$

essentially eliminating the slowest-converging, flat, eigenmode immediately for all $c \leq 1$. The preconditioner defined by Eqs. (26), (27) is the Thick-Cell AP (KAP) [14]. The spectrum for KAP is depicted in Fig. 1 for the 0NIM with an S_4 angular quadrature, $c = 1$, and various cell thicknesses. These spectra illustrate the superb efficiency of KAP for cells thicker than $\sim$5 mfp, a property shared with IDSA [7], but not the FSM–DSA [3]. Nevertheless, KAP's

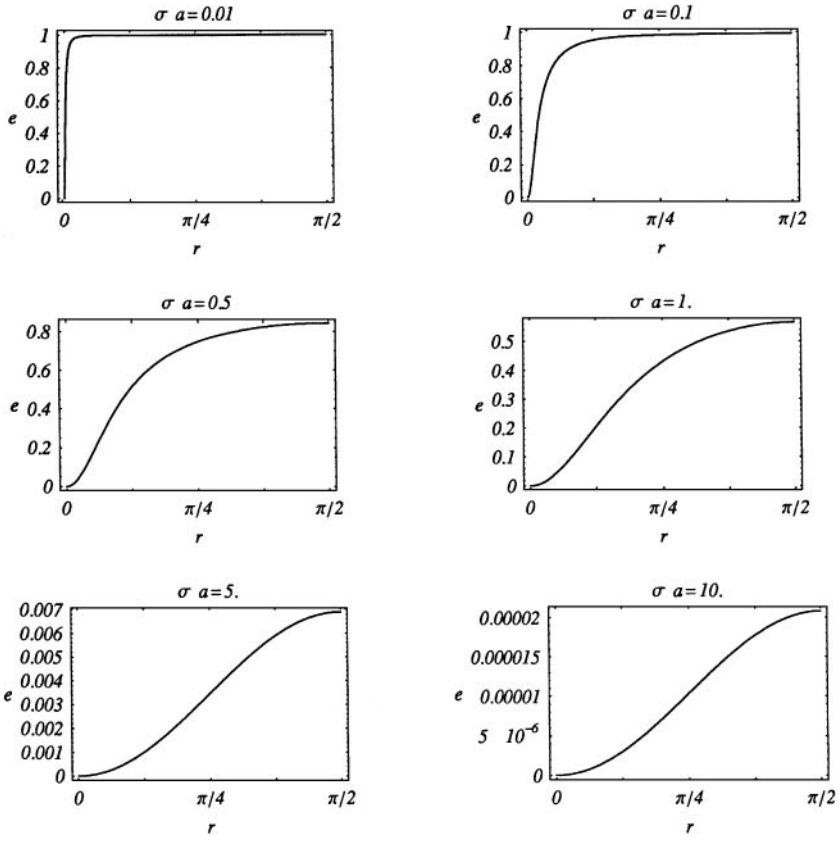

FIG. 1. Spectrum of KAP for the 0NIM with S_4 angular quadrature and $c = 1$.

efficiency, as measured by the smallness of the spectral radius, diminishes with cell size, and for very thin cells loss of stability creeps in.

While the KAP and NAP presented in this and the next sections apply to WDD in general only results for the 0NIM, S_4, $c = 1$ case are reported in the remainder of this section. The spectra for $c < 1$ are generally smaller than those for $c = 1$, and for all c are largely insensitive to the order of the angular quadrature. The spectra of the AP accelerated Step method are qualitatively similar to those of the 0NIM except that the spectral radius does not diminish as rapidly with cell size. Consistent with Reed's results [1] and the IDSA parametric studies reported earlier [7] the AP accelerated DD method becomes unstable for cells thicker than 1.6 and 1.1 mfp for KAP and NAP, respectively. The only conditional stability of the AP for DD is not a disappointing result given the general wisdom that this discretization of the transport operator often becomes inaccurate for cells thicker than $\sim$1 mfp. Similarly, the Step approximation accurately represents the relationship between the edge and cell-average fluxes only for thick cells, i.e., thicker than a few mfp's. The 0NIM spans the entire range of cell sizes because its spatial weights, Eq. (3.c), approach the correct limit, DD or Step, as cell thickness approaches 0 or ∞, respectively.

II.2.b. *Thin-Cell AP for WDD*

The original purpose of the preconditioning technique is to provide an iterative solution alternative to the exact solution algorithm; compare Eqs. (8) and (11). In this work, by

introducing the mesh-sweep flux into the iterative scheme, Eq. (12), we essentially employ this technique as an accelerator to the source iterations represented by the mesh sweeps. This is the reason for the previous iterate flux appearing on the left hand side of Eq. (12), in contrast to the mesh-sweep flux normally used in the corresponding updating equation in standard DSA and IDSA methods. By carefully examining the behavior of the iteration eigenvalue in Eq. (24) as the cell optical thickness approaches zero, we find that, for perfectly scattering problems, $c = 1$,

$$\chi(r) \to \sin^{-2} r, \qquad 0 < r \leq \pi/2, \text{ as } \sigma a \to 0, \tag{28}$$

hence

$$e(r) = \left[1 - \frac{1}{2D_d \sin^2 r}\right] \to 1, \qquad \text{as } \sigma a \to 0, \tag{29}$$

where we used Eqs. (26) and (27). This behavior is verified by the almost flat eigenvalue, $e(r) \sim 1$, r *far* from 0, of this method for thin cells, $\sigma a < 0.1$, displayed in Fig. 1, with the small eigenvalue region near $r = 0$ resulting from the imposed condition for that mode; see Eq. (27).

An easy fix to this behavior is to modify the updating formula, Eq. (12), to

$$\phi^{l+1} - \phi^{l'} = \mathbf{D}^{-1} c(\phi^{l'} - \phi^{l}), \tag{30}$$

which results in error mode decay governed by

$$\Phi^{l+1}(r) = c\left[1 - \chi(r)\sin^2 r - \frac{1 - c + c(\sin^2 r)\chi(r)}{1 - c - 2(1 - c - D_d)\sin^2 r}\right]\Phi^{l}(r). \tag{31}$$

Again we select the D_d parameter so as to effect a zero eigenvalue at $r \to 0$, Eq. (27), to obtain the Thin-cell AP (NAP), whose spectra for the 0NIM with an S_4 angular quadrature, $c = 1$, and various cell thicknesses are plotted in Fig. 2. These spectra show the high efficiency of this preconditioner for all cell thicknesses; nevertheless, comparison with Fig. 1 reveals that for thick cells, KAP provides superior convergence rates.

It is possible to write the NAP formula, Eq. (30), in the form of KAP, Eq. (12), that resembles more closely standard preconditioned iterations where an intermediate iterate, here the mesh sweep flux, does not exist. This can be accomplished by subtracting ϕ^{l} from both sides of Eq. (30) and rearranging to obtain,

$$\phi^{l+1} - \phi^{l} = (\mathbf{I} + \mathbf{D}^{-1} c)(\phi^{l'} - \phi^{l}).$$

This amounts to a KAP whose preconditioner is the full matrix $(\mathbf{I} - \mathbf{D}^{-1}c)^{-1}$. This result might explain why KAP, with only adjacent-cell coupling, does not accelerate problems with thin cells too well. In such cases the coupling among the cells that are not adjacent is too strong to ignore, and only by accounting for this coupling via a full preconditioner like NAP, as well as standard DSA, can effective acceleration be achieved.

II.2.c. *Preconditioners for Non-model 0NIM Problems*

For the benefit of the spectral analyses performed above, all discussions so far have assumed a model problem configuration wherein uniform properties, e.g., size and material

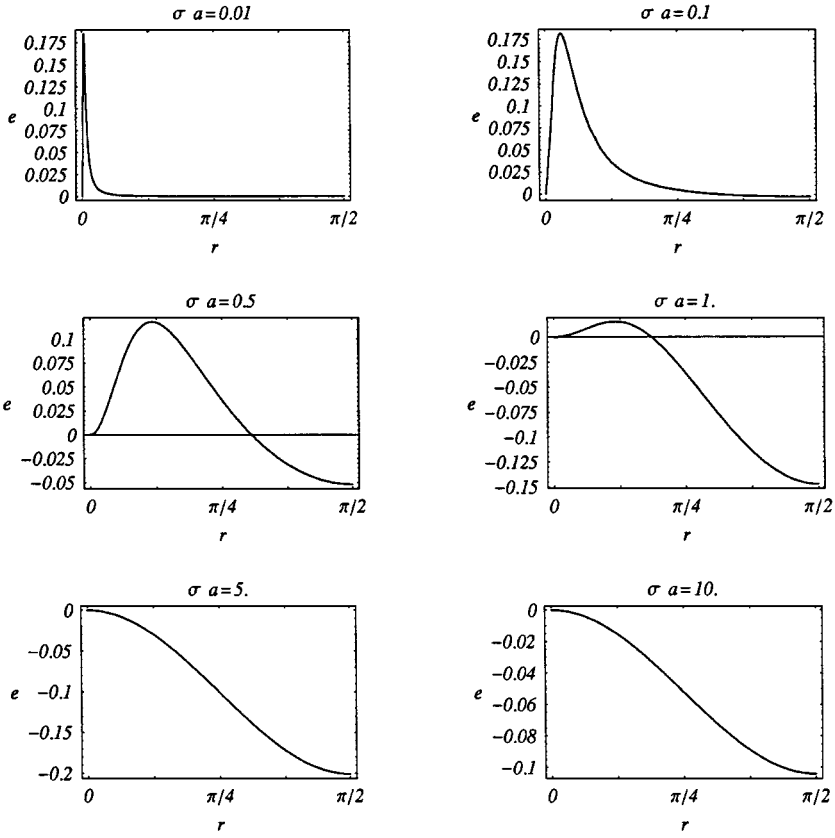

FIG. 2. Spectrum of NAP for the 0NIM with S_4 angular quadrature and $c = 1$.

composition, are assigned to an infinite, or periodic, row of computational cells. In real applications, solved using production codes, cell-property discontinuities are common, and boundary conditions expressing the finite nature of the problem are standard. Therefore, in order to verify the spectral analysis, and establish the utility of the new method in solving real problems, we must provide formulas for the boundary conditions, and for mixing preconditioning methodologies, not only within the same thin/thick cell regime but also across.

The mixing formula must accomplish two functions: compute the effective preconditioner parameters when two adjacent cells have different properties, and adjust the updating formula according to the size of the cell in question. The second function is easily accomplished by testing the cell size against a cut off value, δ, in a Fortran program, and using the mesh-sweep (previous iterate of the) scalar flux for updating, when the cell size is smaller (larger) than δ, respectively. The first function is accomplished in the traditional way of mixing in diffusion theory, namely reciprocal averaging [15] of the *diffusion coefficient*. For example, the equation for cell j becomes

$$-D_o^{+j}(f_{j+1} - f_j) + D_o^{-j}(f_j - f_{j-1}) + (1 - c_j) f_j = \gamma_j \left(\phi_j^{l'} - \phi_j^{l}\right), \qquad (32.a)$$

$$D_o^{\pm j} \equiv \frac{2\sigma_{j\pm1} a_{j\pm1}}{\sigma_{j\pm1} a_{j\pm1}/D_{o,j\pm1} + \sigma_j a_j / D_{o,j}}, \qquad (32.b)$$

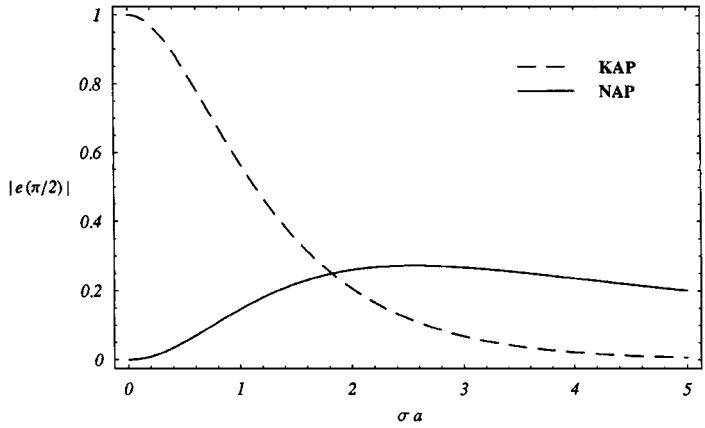

FIG. 3. Spectral radius for KAP (dashed curve) and NAP (solid curve) as a function of σa for the 0NIM with S_4 angular quadrature and $c = 1$.

where $D_{o,j}$ is evaluated from Eqs. (26) and (27) using the local properties of cell j, and

$$\gamma_j = \begin{cases} c_j, & \sigma_j a_j \le \delta, \\ 1, & \sigma_j a_j > \delta. \end{cases} \tag{33}$$

Once the system of equations represented by Eq. (32.a) is solved for f_j, the scalar flux is updated using

$$\phi_j^{l+1} = \begin{cases} \phi_j^{l'} + f_j, & \sigma_j a_j \le \delta, \\ \phi_j^{l} + f_j, & \sigma_j a_j > \delta. \end{cases} \tag{34}$$

To determine the value of the cutoff cell size, δ, we note from comparing Figs. 1 and 2 that for the intermediate cell thickness where the cutoff size occurs, $1 < \sigma a < 5$, the largest eigenvalue is located at $r = \pi/2$. Thus we plot the eigenvalue at that point vs cell thickness in this range for KAP and NAP in Fig. 3. We conclude from Fig. 3 that $\delta \sim 1.8$ for the 0NIM with S_4 angular quadrature and $c = 1$, and use this value for other cases assuming it is not sensitive to the quadrature order or the scattering ratio.

The system of equations, Eqs. (32.a), must be augmented with appropriate expressions for the boundary conditions before it can be solved. For example, for vacuum boundary conditions we use Larsen's recipe [3]. More specifically, a fictitious cell is appended on the left (right) side of the problem external boundaries with nuclear and physical properties identical to those of cell 1 (J) and with cell-average flux residual $\Gamma_1 f_1$ ($\Gamma_J f_J$), respectively [7]. The proportionality factors Γ_j are computed via Larsen's prescription that the edge flux residual is linear in the angular variable μ_n to obtain

$$\Gamma_j = \frac{D_{o,j}\sigma_j a_j/\gamma_j \beta - 1}{D_{o,j}\sigma_j a_j/\gamma_j \beta + 1}, \qquad j = 1, \text{or } J, \tag{35.a}$$

where we have defined

$$\beta \equiv \sum_{n=1}^{N/2} w_n \mu_n. \tag{35.b}$$

Using these expressions in a vacuum boundary condition on the left external edge yields

$$-D_o^{+1} f_2 + \left[D_{o,1}(1-\Gamma_1) + D_o^{+1}\right] f_1 + (1-c) f_1 = \gamma_1\left(\phi_1^{l'} - \phi_1^{l}\right), \tag{36}$$

with an analogous expression for the right external boundary.

II.3. Numerical Verification of 0NIM Theoretical Results

In order to verify the assumptions and hypotheses made in performing the spectral analysis of the new acceleration scheme, as well as the mixing formulas and boundary condition expressions for non-model problems, we implemented our new method, in addition to SI, and FSM–DSA, in the slab geometry WDD computer code AP1D. We use this code to solve the test problem shown in Fig. 4, which is made up of two materials with different optical thicknesses.

The scattering ratio is set to 1 in both materials as this represents the worst case as far as convergence rate is concerned, and the discontinuities in cell properties, namely size and total cross section, are lumped into the dimensionless parameter σa. We independently vary the optical thicknesses of the two materials, $\sigma_1 a_1$ and $\sigma_2 a_2$, between 10^{-5} and 10 to cover a wide range of possible material/mesh discontinuities, and we observe the number of iterations required to achieve 10^{-4} relative pointwise convergence using the standard SI, the FSM–DSA, and the new preconditioned iterations. Table I contains these results; clearly acceleration of some sort is necessary for very thick cells, as is well known. Table I shows the very high efficiency of the preconditioned iterations compared to that of the SI scheme, and its immunity to severe cell-property discontinuities. The results for the new method along the diagonal, $\sigma_1 a_1 = \sigma_2 a_2$, represents the uniform cell-property case, and serves as a verification of the spectral analyses presented above. While the FSM–DSA performs equally well for thin problems, the preconditioned iterations converge faster when thick regions are introduced into the problem. Indeed for very thick problems our new method converges immediately, as predicted by the spectral analysis.

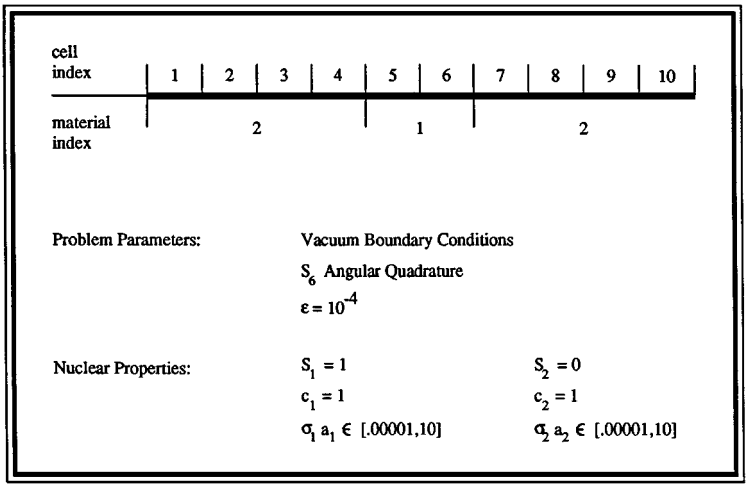

FIG. 4. Configuration for 0NIM test problem.

TABLE I

Number of Iterations[a] Required to Achieve 10^{-4} Relative Pointwise Convergence for the Test Problem Using 0NIM with AP (Top), FSM–DSA (Middle), and SI[b] (Bottom)

	$\sigma_1 a_1$						
$\sigma_2 a_2$	10^{-5}	0.01	0.1	0.5	1	5	10
10^{-5}	1	2	4	4	2	2	1
	1	2	4	5	4	4	4
	2	3	6	17	29	120	215
0.01	3	3	4	4	3	3	3
	3	3	4	5	4	4	4
	4	5	8	18	30	124	222
0.1	5	5	5	5	4	4	4
	5	5	5	5	5	5	5
	15	15	18	29	44	159	279
0.5	4	4	5	4	4	4	4
	5	5	5	5	5	5	5
	67	67	71	88	110	288	477
1	3	3	4	4	3	3	3
	4	4	4	4	4	4	4
	149	149	154	175	203	422	659
5	2	2	3	3	2	2	1
	4	4	4	4	4	3	3
	704	704	709	729	754	956	1199
10	1	2	3	3	2	2	1
	4	4	4	4	4	3	3
	1193	1194	1197	1213	1233	1396	1595

[a] Iteration counter initialized at 0.

[b] Potentially false convergence in cases requring many iterations.

III. ACCELERATION OF THE 1NIM

Early attempts at extending the IDSA formalism to the linear NIM (1NIM) were based on the assumption that the spectral radius depends strongly on the intramoment coupling, but weakly on the intermoment coupling. Had this been the case, it would have allowed acceleration of the zeroth and first spatial moments of the flux to be performed separately with uncoupled standard diffusion operators. This assumption did not materialize, however, and it became necessary to explore preconditioners that include in the preconditioner operator terms that couple the spatial moments of the scalar flux. The resulting AP still possesses a cell-centered diffusion stencil but in the block sense, implying a high probability that standard iterative techniques will be adequate in this case, but that existing diffusion codes cannot be employed as acceleration modules without significant modifications. It is worth noting at this point that the edge-centered FSM–DSA applied in slab geometry to the Linear Discontinuous method (which is comparable to 1NIM) results in a single diffusion equation that must be solved at every acceleration stage for the cell-edge corrections that are then applied to the cell moments of the flux [3]. Clearly this is an advantage of the FSM–DSA over AP in slab geometry that we conjecture will not stand in multidimensional cases where multiple coupled cell-centered diffusion equations could result from FSM–DSA,

and where there are fewer cell-moment discrete variables than cell-edge discrete variables. Another advantage that edge-centered DSA for linear methods in slab geometry possesses is its robustness in the presence of sharp material discontinuities; however, this advantage does not carry over to multidimensional situations where the performance of both edge- and cell-centered acceleration techniques deteriorates in the presence of sharp material discontinuities.

We start this section with a spectral analysis of the uncoupled diffusion operator approach to show its inadequacy regardless of the diffusion parameters employed. We explain this behavior by an asymptotic analysis to show that the elements of the full transport operator that couple the zero and first spatial moments are of the same order as the diagonal elements in the diffusive regime, and thus cannot be neglected. Along the same lines presented for the 0NIM in Section II, we develop KAP and NAP for the 1NIM, which are extremely efficient for corresponding cell thicknesses and describe mixing formulas and boundary conditions for non-model problems. Due to the complexity of the 1NIM only the NAP was implemented in a computer code because it is highly efficient for all cell sizes. We close this section with numerical tests to verify the predicted spectral properties for NAP, and test its robustness in the presence of sharp material and mesh discontinuities.

III.1. Inadequacy of Uncoupled Preconditioners for 1NIM

The 1NIM equations [8] in slab geometry can be written in tensor form,

$$\mathbf{T}^1_{n,j}\left[\psi^{l'}_{n,j}, \psi^{x,l'}_{n,j}, \psi^{o,l'}_{n,j}\right]^T = \mathbf{S}^1_{n,j}\left[\phi^{l}_{j}, \phi^{x,l}_{j}, \psi^{i,l'}_{n,j}\right]^T, \qquad n = 1, \ldots, N;\ j = 1, \ldots, J, \quad (37)$$

where $\psi^{x,l'}_{n,j}$ and $\phi^{x,l}_{j}$ are the linear spatial moments of the nth angular flux residual and the scalar flux residual over the jth computational cell, respectively. The superscript on the matrices in Eq. (37) denotes the 1NIM, and these matrices are given by

$$\mathbf{T}^1_{n,j} \equiv \begin{bmatrix} 1 & 0 & \varepsilon_{n,j}/2 \\ -\mathrm{sg}(\mu_n)\varepsilon_{n,j} & 1 & \mathrm{sg}(\mu_n)\varepsilon_{n,j}/2 \\ \alpha_{n,j} & 3\,\mathrm{sg}(\mu_n) & -(\alpha_{n,j}+1)/2 \end{bmatrix}, \quad (38)$$

$$\mathbf{S}^1_{n,j} \equiv \begin{bmatrix} c_j & 0 & \varepsilon_{n,j}/2 \\ 0 & c_j & -\mathrm{sg}(\mu_n)\varepsilon_{n,j}/2 \\ 0 & 0 & (\alpha_{n,j}-1)/2 \end{bmatrix}, \quad (39)$$

where for the 1NIM, the spatial weights are given by [8]

$$\alpha_{n,j} = [\coth(1/\varepsilon_{n,j}) - \varepsilon_{n,j}]^{-1} - 3\varepsilon_{n,j}. \quad (40)$$

All other terms are as defined in Section II. The equations represented by the first and second rows of Eq. (37) stand for the balance condition on the zeroth and first spatial moments of the angular flux residual, respectively, while the third row stands for the weighted difference relation, where the incoming angular flux residual has been moved to the RHS as in Eq. (4).

Applying two uncoupled *diffusive* preconditioners to the zeroth and first spatial moments of the scalar flux residuals governed by the square of the dimensionless diffusion length,

Δ^{ν}, yields the system

$$-\Delta^{\nu}\left(f_{j+1}^{\nu}-2f_{j}^{\nu}+f_{j-1}^{\nu}\right)+(1-c)f_{j}^{\nu}=c\left(\phi_{j}^{\nu,l'}-\phi_{j}^{\nu,l}\right). \tag{41}$$

The preconditioning stage is then followed by the updating formula

$$\phi_{j}^{\nu,l+1}=\phi_{j}^{\nu,l'}+f_{j}^{\nu},\qquad \nu=\text{null},x. \tag{42}$$

In Eq. (41) we assume a model problem configuration, thus suppressing the cell index on the scattering ratio and Δ^{ν}. The attractiveness (simplicity) of this method is evident from Eq. (41); the system of equations that must be solved in the acceleration stage is decoupled into two sets, each of which is a regular, cell-centered discretization of the diffusion equation, that can be solved using existing efficient algorithms and codes. The question, however, is whether there exists a choice of Δ^{ν} that makes the iterative scheme represented by Eqs. (37), (41), and (42) unconditionally stable and rapidly convergent.

We augment the Fourier decomposition in Eqs. (21) with

$$\phi_{j}^{x,l}=\Phi^{x,l}\exp[\hat{\imath}\lambda x_{j}], \tag{43.a}$$

$$\psi_{n,j}^{x,l'}=\Psi_{n}^{x,l'}\exp[\hat{\imath}\lambda x_{j}], \tag{43.b}$$

$$\phi_{j}^{x,l'}=\Phi^{x,l'}\exp[\hat{\imath}\lambda x_{j}], \tag{43.c}$$

$$f_{j}^{\nu}=F^{\nu}\exp[\hat{\imath}\lambda x_{j}],\qquad \nu=\text{null},x, \tag{43.d}$$

and substitute into Eqs. (37), (41), and (42). After some manipulation of the decomposed equations we obtain the Fourier representation of the mapping of the error modes by the mesh-sweep process

$$\mathbf{\Phi}^{l'}=c\chi^{x}(r)\mathbf{\Phi}^{l}, \tag{44}$$

where we defined the vector $\mathbf{\Phi}^{k}\equiv[\Phi^{k},\Phi^{x,k}]^{T}$, $k\equiv l$, or l', and

$$\chi^{x}(r)\equiv\begin{bmatrix}1-\xi_{1}(r)\sin^{2}r & -\frac{3\hat{\imath}}{2}\xi_{2}(r)\sin(2r)\\ \frac{\hat{\imath}}{2}\xi_{2}(r)\sin(2r) & 1-3\xi_{2}(r)\cos^{2}r-3\xi_{3}(r)\sin^{2}r\end{bmatrix}, \tag{45}$$

$$\xi_{1}(r)\equiv\sum_{n=1}^{N}w_{n}\frac{\varepsilon_{n}(\alpha_{n}+3\varepsilon_{n})[1+\varepsilon_{n}(\alpha_{n}+3\varepsilon_{n})]}{(\alpha_{n}+3\varepsilon_{n})^{2}\cos^{2}r+[1+\varepsilon_{n}(\alpha_{n}+3\varepsilon_{n})]^{2}\sin^{2}r}, \tag{46.a}$$

$$\xi_{2}(r)\equiv\sum_{n=1}^{N}w_{n}\frac{\varepsilon_{n}(\alpha_{n}+3\varepsilon_{n})}{(\alpha_{n}+3\varepsilon_{n})^{2}\cos^{2}r+[1+\varepsilon_{n}(\alpha_{n}+3\varepsilon_{n})]^{2}\sin^{2}r}, \tag{46.b}$$

$$\xi_{3}(r)\equiv\sum_{n=1}^{N}w_{n}\frac{\varepsilon_{n}^{2}[1+\varepsilon_{n}(\alpha_{n}+3\varepsilon_{n})]}{(\alpha_{n}+3\varepsilon_{n})^{2}\cos^{2}r+[1+\varepsilon_{n}(\alpha_{n}+3\varepsilon_{n})]^{2}\sin^{2}r}, \tag{46.c}$$

and where we have assumed symmetry of the angular quadrature. Equation (44) is the 1NIM analogue of Eq. (22), and the superscript on χ^{x} indicates that it is the 1NIM mapping that governs the evolution of the unaccelerated iterates' eigenmodes.

Fourier analysis of the diffusion equations, Eq. (41), produces an expression which when substituted in the Fourier decomposition of Eq. (42) yields the mapping of the error modes for the preconditioned system

$$\mathbf{\Phi}^{l+1} = c\left\{\chi^x + \begin{bmatrix} 1/(1-c+4\Delta\sin^2 r) & 1/(1-c+4\Delta\sin^2 r) \\ 1/(1-c+4\Delta^x\sin^2 r) & 1/(1-c+4\Delta^x\sin^2 r)\end{bmatrix}[c\chi^x - \mathbf{I}]\right\}\mathbf{\Phi}^l. \quad (47)$$

Attenuation of the accelerated residual modes is determined by the spectrum of the matrix on the RHS of Eq. (47). It is straightforward to show that for $c = 1$, one of the eigenvalues of this matrix diverges as r^{-2} when $r \to 0$ regardless of Δ^v, thereby establishing the inadequacy of this iterative method.

III.2. Adjacent-Cell Preconditioners for 1NIM

In order to understand the reason for the inadequacy of preconditioners that lack the coupling between the zeroth and first spatial moments of the flux we compute the exact multidiagonal preconditioner, **B** matrix, for the 1NIM (in this case a *block* matrix). Through an asymptotic analysis analogous to that conducted in Section II.1 we can then determine the relative importance of this coupling in the limit of diffusive regimes. Since the procedure is identical to the one detailed in Section II.1 we skip to the final result,

$$\mathbf{B}^1_{j,j} = \mathbf{I} - c\sum_{n=1}^{N}\frac{w_n}{1+(\varepsilon_n+1)(\alpha_n+3\varepsilon_n)}\begin{bmatrix}1+(\alpha_n+3\varepsilon_n) & 0\\ 0 & 1+\alpha_n(\varepsilon_n+1)\end{bmatrix}, \quad (48.a)$$

$$\mathbf{B}^1_{j,j\pm1} = -c\sum_{n=1}^{N}\frac{w_n}{[1+(\varepsilon_n+1)(\alpha_n+3\varepsilon_n)]^2}\begin{bmatrix}\varepsilon_n(\alpha_n+3\varepsilon_n)^2 & \pm3\varepsilon_n(\alpha_n+3\varepsilon_n)\\ \mp\varepsilon_n(\alpha_n+3\varepsilon_n) & -3\varepsilon_n\end{bmatrix}, \quad (48.b)$$

$$\mathbf{B}^1_{j,j\pm2} = -c\sum_{n=1}^{N}\frac{w_n[1+(\varepsilon_n-1)(\alpha_n+3\varepsilon_n)]}{[1+(\varepsilon_n+1)(\alpha_n+3\varepsilon_n)]^3}\begin{bmatrix}\varepsilon_n(\alpha_n+3\varepsilon_n)^2 & \pm3\varepsilon_n(\alpha_n+3\varepsilon_n)\\ \mp\varepsilon_n(\alpha_n+3\varepsilon_n) & -3\varepsilon_n\end{bmatrix}, \quad (48.c)$$

where the superscript on $\mathbf{B}^1$ denotes the 1NIM. In Eqs. (48) we have assumed uniform cell properties by suppressing the cell index on the preconditioner parameters, and we assumed symmetry of the angular quadrature.

It is clear from Eqs. (48) that while the diagonal block exactly decouples the zero and first moments of the scalar flux, the off-diagonal blocks do not. Indeed, an asymptotic analysis of the exact preconditioner blocks in the limit of thick computational cells yields

$$\mathbf{B}^1_{j,j} = (1-c)\mathbf{I} + \frac{c}{\sigma a}\sum_{n=1}^{N} w_n|\mu_n|\begin{bmatrix}1 & 0\\ 0 & 3\end{bmatrix} + O(\sigma a)^{-2}, \quad (49.a)$$

$$\mathbf{B}^1_{j,j\pm1} = -\frac{c}{2\sigma a}\sum_{n=1}^{N} w_n|\mu_n|\begin{bmatrix}1 & \pm3\\ \mp1 & -3\end{bmatrix} + O(\sigma a)^{-2}, \quad (49.b)$$

$$\mathbf{B}^1_{j,j\pm2} = -\frac{c}{(\sigma a)^3}\sum_{n=1}^{N} w_n|\mu_n|^3\begin{bmatrix}1 & \pm3\\ \mp1 & -3\end{bmatrix} + O(\sigma a)^{-4}. \quad (49.c)$$

Equations (49) agree with the 0NIM result that when $c \sim 1$ the first off-diagonal blocks are of the same order as the diagonal block, and thus cannot be ignored even for very thick

computational cells; blocks farther from the diagonal vanish faster as $\sigma a \to \infty$. The most important feature of the exact preconditioner that is illustrated by Eqs. (49) is the fact that the terms coupling the zeroth and first spatial moments of the scalar flux in the off-diagonal blocks are $O(\sigma a)^{-1}$, the same order as the diagnoal block and the other elements of the off-diagonal block. This explains the poor spectral properties of preconditioners that ignore this coupling.

III.2.a. *Thick-Cell AP for 1NIM*

To proceed with the derivation of KAP for 1NIM we introduce a Fourier decomposition of the generic block-AP to obtain the mapping of the error modes by the accelerated scheme

$$\mathbf{\Phi}^{l+1} = [\mathbf{I} + \mathbf{D}^{-1}(c\chi^x - \mathbf{I})]\mathbf{\Phi}^l, \tag{50.a}$$

where the Fourier-decomposed generic KAP is

$$\mathbf{D}(r) \equiv \begin{bmatrix} D_0 & 0 \\ 0 & D_1 \end{bmatrix} + 2\begin{bmatrix} D_{0,0}\cos(2r) & \hat{\imath} D_{0,1}\sin(2r) \\ \hat{\imath} D_{1,0}\sin(2r) & D_{1,1}\cos(2r) \end{bmatrix}, \tag{50.b}$$

and χ^x is given by Eq. (45). Note that in Eq. (50.a) the KAP updating formula, i.e., with respect to the lth iterate, is used.

Since the details of the derivations of KAP and NAP are the same, and because only the NAP is implemented and tested for 1NIM, we briefly outline the derivation of KAP and elaborate on the analogous details in the following section. Removing the singularity in the spectrum of KAP at the origin in Fourier space results in a stability condition that relates the elements of the diagonal and off-diagonal blocks of $\mathbf{D}$. Even then, there are sufficient degrees of freedom to permit imposing two conditions on the spectrum, and we choose these to be that the KAP eigenvalues vanish in the limit $r \to 0$, and at $r = \pi/2$, an idea reminiscent of the approach introduced in Ref. [5] for the DD discretization of the transport equation. This procedure leads to the following expressions for the KAP elements appearing in Eq. (50.b),

$$D_0 = 1 - c + \frac{c\xi_1(\pi/2)}{2}, \tag{51.a}$$

$$D_1 = 1 - c + \frac{3c}{2}[\xi_2(0) + \xi_3(\pi/2)], \tag{51.b}$$

$$D_{0,0} = -\frac{c}{4}\xi_1(\pi/2), \tag{51.c}$$

$$D_{0,1} = \frac{3c}{4}\xi_2(0), \tag{51.d}$$

$$D_{1,0} = \frac{[1 - c + 3c\xi_2(0)][\xi_1(0) - \xi_1(\pi/2)] - 3c[\xi_2(0)]^2}{12\xi_2(0)}, \tag{51.e}$$

$$D_{1,1} = \frac{3c}{4}[\xi_2(0) - \xi_3(\pi/2)]. \tag{51.f}$$

The spectrum of the 1NIM, $e(r)$, comprises two eigenvalues per Fourier mode r. Since the rate of convergence is dictated by the eigenvalue of the larger magnitude over the Fourier space, we are particularly interested in $\sup|e|$, where the sup is over the two eigenvalues

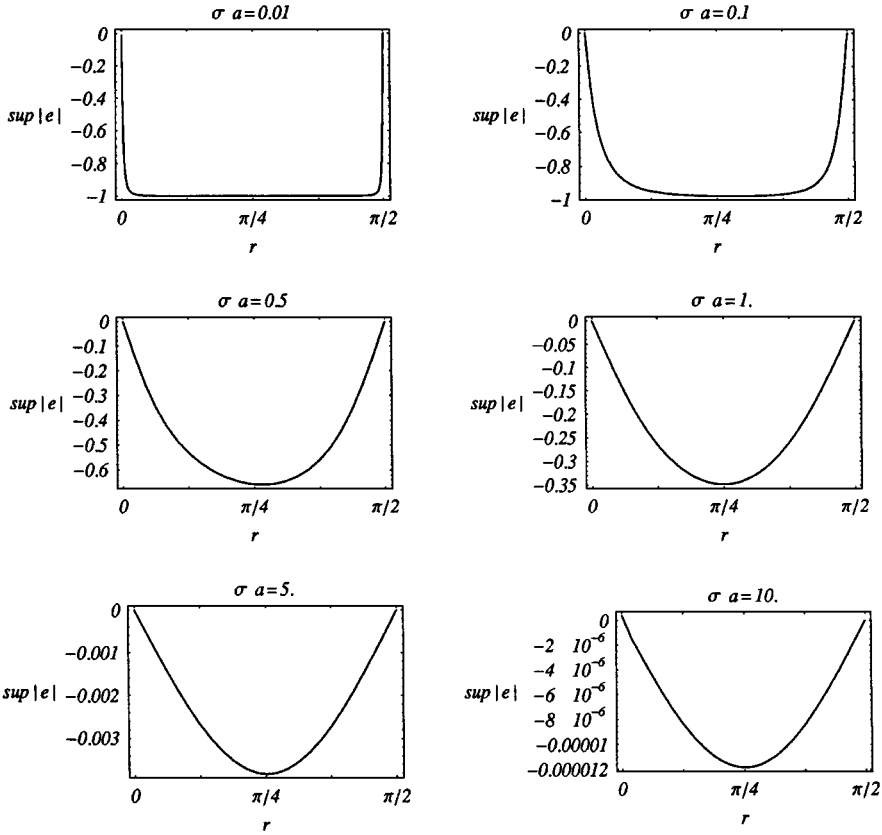

FIG. 5. Spectra of KAP for the 1NIM with S_4 angular quadrature and $c = 1$.

at r; we loosely refer to this as *spectrum* in the following discussion. Spectra for the KAP iterative method are shown in Fig. 5 for the 1NIM with S_4 angular quadrature, $c = 1$, and various cell optical thicknesses. In these plots we assign a negative value to $\sup|e|$ if the eigenvalues are complex. Note the complex spectra for all $r \in [0, \pi/2]$ and for all values of σa a depicted in Fig. 5. The spectra shown in Fig. 5 resemble their 0NIM counterparts depicted in Fig. 1 with two significant differencs. First, the high frequency eigenmodes, $r = \pi/2$, converge immediately here as required by the condition imposed in the derivation of the KAP elements. Second, the spectral radius of the 1NIM KAP is generally smaller than that of the 0NIM KAP, and for very thick cells, $\sigma a \geq 10$, it is almost an order of magnitude smaller. Nevertheless, this method still lacks the necessary efficiency for computational cells of thin and intermediate thickness, thus motivating derivation of a NAP for 1NIM in the next section.

III.2.b. *Thin-Cell AP for 1NIM*

The development of thin-cell AP, NAP, for the 1NIM follows essentially the same pattern established by the 0NIM development as described in Section II.2.b. Specifically, we alter the updating formula to make the update with respect to the mesh-sweep scalar flux instead of the previous iterate. Through a Fourier decomposition the error mode mapping is described

by an expression similar to Eq. (50.a) but with the first identity matrix, **I**, appearing on the RHS replaced by $c\chi^x$, to obtain

$$\mathbf{N}(r) = c[\chi^x(r) + \mathbf{D}^{-1}(r)\{\chi^x(r) - \mathbf{I}\}], \tag{52}$$

which maps the eigenmodes of the NAP-accelerated residual iterates. If one takes the limit of **N** as $r \to 0$ and requires the diagonal elements to approach zero while the off-diagonal elements remain bounded, a sufficient condition for the flat mode eigenvalue to vanish yields the formulas

$$D_{0,0} = \frac{1 - c - D_0}{2}, \tag{53.a}$$

$$D_{1,0} = \frac{D_1 + 2D_{1,1}}{8D_{0,1}}\left[1 - c - D_0 + \frac{1}{2}\xi_1(0)\right] - \frac{c}{4}\xi_2(0), \tag{53.b}$$

$$D_{0,1} = \frac{3\xi_2(0)}{4}\frac{D_1 + 2D_{1,1}}{1 - c[1 - 3\xi_2(0)]}, \tag{53.c}$$

$$D_{1,1} = \frac{1}{2}\left[\frac{1}{1 - 3\xi_2(0)} - c - D_1\right]. \tag{53.d}$$

Similar to the KAP case, here also we have enough preconditioner parameters to require the iteration eigenvalues to vanish at $r = \pi/2$, to obtain the conditions

$$D_0 = 1 - c + \frac{1}{2}\frac{\xi_1(\pi/2)}{1 - \xi_1(\pi/2)}, \tag{54.a}$$

$$D_1 = 2D_{1,1} - c + \frac{1}{1 - 3\xi_3(\pi/2)} = \frac{1}{2}\left[\frac{1}{1 - 3\xi_3(\pi/2)} + \frac{1}{1 - 3\xi_2(0)}\right] - c. \tag{54.b}$$

Equations (54) can be substituted in Eqs. (53) to obtain explicit expressions for all the NAP parameters if desired.

Spectra of the 1NIM NAP with S_4 angular quadrature, $c = 1$, and various cell optical thicknesses are plotted in Fig. 6, where negative values of $\sup|e|$ imply complex eigenvalues at a given r. The discontinuities in the spectra in Fig. 6 with $\sigma a = 0.1$ and 0.5 indicate points of transition from real to complex spectra. These spectra exhibit excellent spectral properties, and bear a strong resemblance to their 0NIM counterparts. While the NAP provides an unconditionally stable, rapidly convergent iterative scheme for all cell thicknesses, it is less efficient than the KAP for computational cells thicker than ~5 mfp, where KAP converges extraordinarily fast. Nevertheless, the complexity of the mixing process in this higher order method precludes combining KAP and NAP into a conditional preconditioner as has been accomplished for the 0NIM; hence only the NAP is implemented and tested as described in Section III.3.

III.2.c. *Preconditioners for Non-model 1NIM Problems*

In order to determine the mixing formula for the 1NIM NAP we extended the standard approach used to derive the reciprocal averaging formula to include the linear spatial moment of the flux also [15]. This results in reciprocal averaging formulas for each of the elements

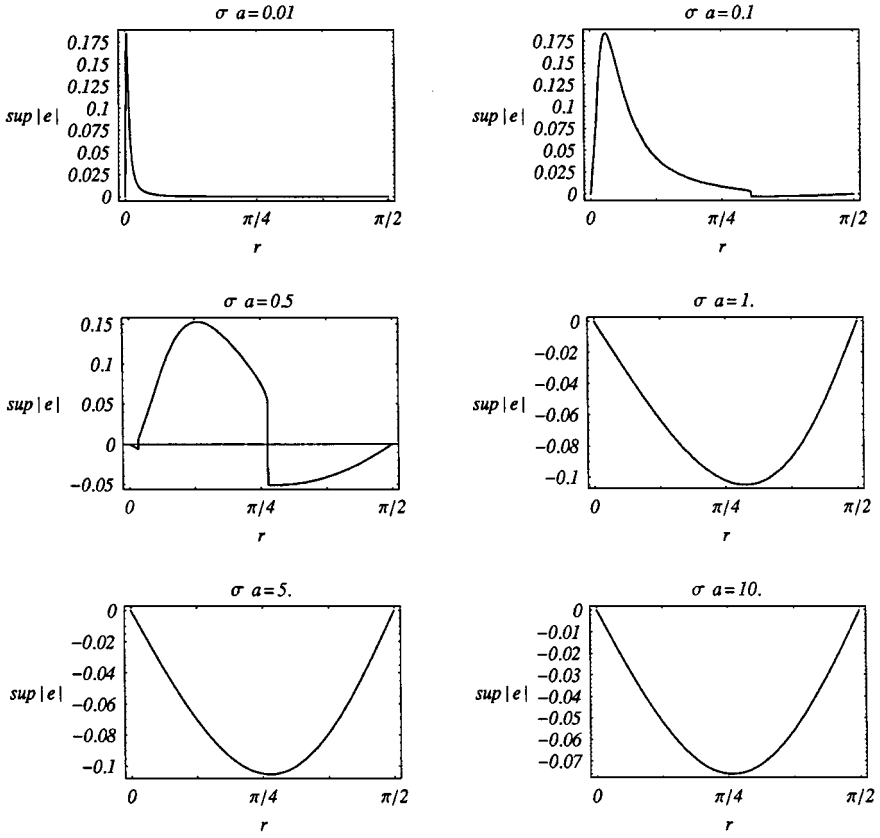

FIG. 6. Spectra of NAP for the 1NIM with S_4 angular quadrature and $c = 1$.

of the AP generally along the same lines as Eq. (32.a),

$$-\begin{bmatrix} D^{+j}_{0,0} & D^{+j}_{0,1} \\ D^{+j}_{1,0} & D^{+j}_{1,1} \end{bmatrix} \begin{bmatrix} f_{j+1} - f_j \\ f^x_{j+1} - f^x_j \end{bmatrix} + \begin{bmatrix} D^{-j}_{0,0} & -D^{-j}_{0,1} \\ -D^{-j}_{1,0} & D^{-j}_{1,1} \end{bmatrix} \begin{bmatrix} f_j - f_{j-1} \\ f^x_j - f^x_{j-1} \end{bmatrix}$$
$$+ \begin{bmatrix} 1 - c_j & 0 \\ 0 & D_{1,j} - 2D_{1,1,j} \end{bmatrix} \begin{bmatrix} f_j \\ f^x_j \end{bmatrix} = c_j \begin{bmatrix} \phi^{l'}_j - \phi^l_j \\ \phi^{x,l'}_j - \phi^{x,l}_j \end{bmatrix}, \tag{55}$$

where $D^{\pm j}_{i,i'}$ are defined in analogy to Eq. (32.b). Since only NAP is considered here the updating formula is with respect to the mesh-sweep flux, $\phi^{\nu,l'}_j$, $\nu \equiv$ null, x.

The boundary conditions for the 1NIM AP are also derived in analogy to the 0NIM case wherein the zeroth and first spatial moments of the scalar flux in the fictitious cells to the left and right boundaries of the problem are expressed as $\Gamma_1 f^\nu_1$ and $\Gamma_J f^\nu_J$, $\nu \equiv$ null, x, respectively, where Γ_j, $j = 1$ or J, are given by Eq. (35.a).

III.3. Numerical Verification of 1NIM Theoretical Results

In order to test the validity of the assumptions and hypotheses made in performing the spectral analysis presented above, and to demonstrate the efficiency of the developed preconditioners we upgraded the test code AP1D described in Section II.3 to include the

TABLE II

Number of Iterations[a] Required to Achieve 10^{-4} Relative Pointwise Convergence for the Test Problem Using 1NIM with AP (Top), and SI[b] (Bottom)

	$\sigma_1 a_1$						
$\sigma_2 a_2$	10^{-5}	0.01	0.1	0.5	1	5	10
10^{-5}	2	3	4	5	6	5	5
	2	3	6	17	32	215	558
0.01	3	4	4	5	5	100[c]	100[c]
	4	5	8	18	33	218	562
0.1	6	6	6	7	8	24	40
	15	15	18	29	45	242	597
0.5	6	6	7	6	6	12	19
	69	70	74	91	115	355	746
1	7	6	8	6	5	7	11
	170	171	176	201	232	524	936
5	6	100[c]	23	13	8	4	4
	1682	1683	1693	1739	1797	2256	2804
10	5	100[c]	40	21	12	5	4
	4040	4042	4052	4098	4156	4610	5133

[a] Iteration counter initialized at 0.

[b] Potentially false convergence in cases requring many iterations.

[c] Did not converge in 100 iterations.

1NIM. To verify the spectral analysis, mixing formula, and boundary conditions for the 1NIM NAP we solved the same suite of test problems shown in Fig. 4 with the new acceleration method and SI. It is important to note that unlike many implementations of high order transport methods, the convergence criterion is applied here to both spatial moments of the scalar flux, not just the average flux. The results of these numerical experiments are shown in Table II. The number of iterations for AP along the diagonal, i.e., $\sigma_1 a_1 = \sigma_2 a_2$, is in excellent agreement with the spectral analysis graphically depicted in Fig. 6. However, some of the cases with sharp material discontinuities consume more iterations than can be justified by the analysis, and a few do not converge at all. These peculiar cases might in fact be a consequence of a larger pattern observed in multidimensional geometries and at present under investigation [16]. Namely, there is strong evidence that there do not exist unconditionally stable and robust preconditioners with a cell-centered diffusion coupling stencil for problems with sharp mesh and material discontinuities. In any case, it is evident from the results shown in Table II that AP converges over a large region in parameter space, and that when it does it saves many inner iterations required for convergence by SI.

IV. CONCLUSION

We applied the preconditioning technique to neutral particle transport methods with the purpose of accelerating iterative convergence. Preconditioning provides a general framework for studying the spectral properties of a wide variety of acceleration techniques, like the standard Jacobi, SOR, etc., methods of numerical analysis, linear DSA methods studied extensively in the nuclear field, or novel non-traditional operators. Indeed, unlike DSA, where

the diffusion operator naturally arises from taking the P_1 approximation of the discrete-variable transport equation, when we focus on preconditioners that operate on the spatial moments of the scalar flux we *derive* the discretized diffusion equation as a special case of a general necessary condition for stability. Such preconditioners couple adjacent cells, hence the term Adjacent-Cell Preconditioners (AP), in a cell-centered diffusion coupling stencil that is easy and efficient to solve by most available diffusion codes. In addition, because AP is cell-centered it involves fewer discrete variables when extended to multidimensional geometry or higher order spatial approximations than the corresponding edge-centered or point-centered methods.

In this paper we derived AP in slab geometry for a class of lowest order methods characterized by the WDD formula and for the first-order Nodal method 1NIM. Spectral analysis of the AP-accelerated methods on model problem configurations illustrates its unconditional stability and effectiveness in reducing the number of iterations required for convergence. Indeed, the spectral radius vanishes in the limit of very thick computational cells, the cases most needing of acceleration, implying immediate convergence. Testing of our new technique in a suite of test problems designed to cover a wide range in parameter space, and including material discontinuity, demonstrates its efficiency in slab geometry for all WDD cases and most 1NIM cases.

The focus in this paper has been on the efficiency of the acceleration method, not on the accuracy of the solution obtained; since AP converges to the same solution as the unaccelerated scheme (see Eq. (12)), the assumption is that the user has selected the best mesh to balance accuracy with computational efficiency. The reader is reminded that because WDD methods, including 0NIM, do not possess the thick diffusion limit of the transport equation their local accuracy deteriorates significantly for thick cells where AP has the greatest advantage. In contrast, 1NIM preserves the thick diffusion limit behavior of the transport equation; hence it can provide highly accurate solutions at increasing computational efficiency with increasing cell size.

We have already extended the AP approach to multidimensional Cartesian geometry and implemented the resulting method in the three dimensional production transport code TORT [17]. The multidimensional AP has essentially the same excellent spectral properties for model problems as its slab geometry counterpart. However, attempts to achieve unconditional robustness in problems with sharp mesh and material discontinuities have failed [18], and recently have been proven to be mathematically impossible to achieve [16]. We conjecture that the lack of unconditional stability of the AP for 1NIM with material discontinuity is related to this fact. It would be interesting to explore nontraditional preconditioners in pursuit of this goal.

ACKNOWLEDGMENT

The author thanks Professor Marvin Adams for valuable discussions.

REFERENCES

1. W. H. Reed, The effectiveness of acceleration techniques for iterative methods in transport theory, *Nucl. Sci. Eng.* **45**, 245 (1971).
2. R. E. Alcouffe, Diffusion synthetic acceleration methods for the diamond-differenced discrete ordinates equations, *Nucl. Sci. Eng.* **64**, 344 (1977).

3. E. W. Larsen, Unconditionally stable diffusion synthetic acceleration methods for the slab geometry discrete ordinates equations. I. Theory, *Nucl. Sci. Eng.* **82**, 47 (1982).
4. D. R. McCoy and E. W. Larsen, Unconditionally stable diffusion synthetic acceleration methods for the slab geometry discrete ordinates equations. II. Numerical results, *Nucl. Sci. Eng.* **82**, 64 (1982).
5. E. M. Gelbard and H. Khalil, Alternative differencing technique for the synthetic method, *Trans. Am. Nucl. Soc.* **45**, 322 (1983).
6. H. Khalil, Effectiveness of a consistently formulated diffusion-synthetic acceleration differencing approach, *Nucl. Sci. Eng.* **98**, 226 (1988).
7. Y. Y. Azmy, Cell-centered imposed diffusion synthetic acceleration for weighted difference transport methods, *Nucl. Sci. Eng.* **115**, 265 (1993).
8. Y. Y. Azmy, The weighted diamond difference form of nodal transport methods, *Nucl. Sci. Eng.* **98**, 29 (1988).
9. J. M. Ortega, *Numerical Analysis: A Second Course* (SIAM, Philadelphia, 1990).
10. L. A. Hageman and D. M. Young, *Applied Iterative Methods* (Academic Press, New York, 1981).
11. Y. Y. Azmy, Post-convergence automatic differentiation of iterative schemes, *Nucl. Sci. Eng.* **125**, 12 (1997).
12. Y. Y. Azmy, A new algorithm for generating highly accurate benchmark solutions to transport test problems, in *Proceedings, XI ENFIR / IV ENAN Joint Nuclear Conference, Pocos de Caldas Springs, MG, Brazil, August 18–22, 1997*; on CD-ROM (1997).
13. W. A. Rhoades and D. B. Simpson, *The TORT Three-Dimensional Discrete Ordinates Neutron/Photon Transport Code*, ORNL / TM-13221 (1997).
14. Y. Y. Azmy, Adjacent-cell preconditioners for solving optically thick neutron transport problems, in *Proceedings, Eighth International Conference on Radiation Sheilding, Arlington, Texas, April 24–27, 1994* (Am. Nucl. Soc., La Grange Park, IL, 1994), Vol. I, p. 193.
15. S. Nakamura, *Computational Methods in Engineering and Science* (Wiley, New York, 1977).
16. Y. Y. Azmy, Impossibility of unconditional stability and robustness of diffusive acceleration schemes, in *Proceedings, 1998 ANS Topical Meeting on Radiation Protection and Shielding, Nashville, TN, April 19–23, 1998* (Am. Nucl. Soc., La Grange Park, IL, 1998), Vol. 1, p. 480.
17. Y. Y. Azmy, Adjacent-cell preconditioners for accelerating multidimensional neutron transport methods, in *Proceedings, Conference on Advances and Applications in Radiation Protection and Shielding, N. Falmouth, MA, April 21–25, 1996* (Am. Nucl. Soc., La Grange Park, IL, 1996), Vol. 1. p. 390.
18. Y. Y. Azmy, Analysis and performance of adjacent-cell preconditioners for accelerating multidimensional transport calculations, in *Proceedings, OECD/NEA Meeting on 3D Deterministic Radiation Transport Computer Programs, Features, Applications, and Perspectives, Paris, France, December 2–3, 1996* (Organization for Economic Cooperation and Development, Paris, 1997), p. 197.